Synergetic pinning centres in $BaZrO_3$-doped $YBa_2Cu_3O_{7-x}$ films induced by $SrTiO_3$ nano-layers.

A.Crisan[1,2,*], V.S. Dang[2,3], P. Mikheenko[2,4], A.M. Ionescu[1,5], I.Ivan[1], L. Miu[1]

[1] *National Institute for Materials Physics Bucharest, 405A Atomistilor Str., 077125 Magurele, Romania*

[2] *School of Metallurgy and Materials, University of Birmingham, Edgbaston, B15 2TT Birmingham, UK*

[3] *Nano and Energy Center, VNU Hanoi University of Science, 334 Nguyen Trai, Thanh Xuan, Hanoi, Vietnam*

[4] *Department of Physics, University of Oslo, P.O. Box 1048 Blindern, N-0316 Oslo, Norway*

[5] *University of Bucharest, Faculty of Physics 077125 Bucharest-Magurele, Romania*

[*]Corresponding author: adrian.crisan@infim.ro; acrisan652@gmail.com

Abstract

We report an enhancement of critical current density (J_c) and unusual behaviour of its dependence on field orientation in $YBa_2Cu_3O_{7-x}$ (YBCO) nanostructured films by a combination of substrate decoration with Ag nano-dots, of incorporation of $BaZrO_3$ (BZO) nano-particles and nano-rods, and of multilayer architecture (a thin $SrTiO_3$ layer separating two 1.5 μm-thick YBCO layers). $SrTiO_3$ insulating layers were 15, 30 or 45 nm thick. The highest improvement of J_c in applied magnetic fields smaller than 1 T occurs in the bi-layer with 30 nm thick STO, while a 45 nm layer of $SrTiO_3$ gives highest J_c in fields higher than 1 T. Our thick nanostructured films show significant improvement of J_c in magnetic field along both the *c* axis and the *ab*-plane direction. The presence of BZO nano-rods, *ab*-plane defects and nano particles of BZO and Y_2O_3 was observed in Transmission Electron Microscopy (TEM) images of the film. The peculiarities of artificial pinning centres revealed in the TEM images of the nanostructured films are used to explain an unusual split of the peak in the J_c dependence on the magnetic field along the *ab*-plane of YBCO. Effective pinning potentials in high magnetic fields have rather high values for such thick films.

PACS: 74.78.Fk; 74.25.Sv; 74.25.Wx; 68.37.Lp

Keywords: superconducting films; multilayers; nanoscale defects; artificial pinning centres; critical current; current anisotropy

1. Introduction

Large scale power applications of $YBa_2Cu_3O_{7-x}$ (YBCO) films processed as long-length coated superconductors depend on the development of low-cost methods for the preparation of thick films with high critical current density (J_c) to obtain high critical current per centimetre of width ($I_{c\text{-}w}$) [1]. For applications in moderate and high magnetic fields, high J_c and $I_{c\text{-}w}$ values require high density of defects (pinning centres, both natural and artificial) preventing motion of magnetic flux induced by Lorentz force and thermal energy. First methods like substrate decoration [2-4] or deposition from composite target, e.g. of YBCO with $BaZrO_3$ (BZO) nanoinclusions [5] or with $Gd_2Ba_4CuWO_y$ [6] were targeting one specific type of pinning centres. The improvement of J_c could be further increased by the proper choice of the architecture of the films, e.g. using a multilayer structure in which YBCO layers are separated by thin insulating layer such as CeO_2 [7]. Recent approaches are targeting several types of pinning centres by using double-doping, for example, with BZO and Y_2O_3 [8, 9], or Gd_3TaO_7 and YBa_2NbO_6 [10]. More recently, large pinning force and matching effects were reported by addition of mixed double perovskite $Ba_2Y(Nb/Ta)O_6$ which resulted in an unusual pinning landscape consisting in $Ba_2(Y/Gd)(Nb/Ta)O_6$ segmented nano-rods parallel to the *c*-axis and $(Y/Gd)_2O_3$ plate-like nanoparticles parallel to the *a*-*b* plane [11]

This paper reports the combination of the three methods: substrate decoration, BZO nano-inclusions and multilayer architecture that brings together the advantages of each approach, creating a very complex landscape of synergetic pinning centres. By combination of substrate decoration with Ag nano-dots (that proved to promote columnar growth of YBCO [12]) with BZO-doping [13], BZO nano-rods and nanoparticles act as effective pinning centres for magnetic field in both directions: along the *c* axis and in the *ab*-plane. Additional defects were created in YBCO by the $SrTiO_3$ (STO) nanoscale layer near the interfaces; this multilayer architecture provides additional strong pinning along the *ab*-plane, as in Ref. [14].

2. Experimental

Ag nano-dots were deposited on the STO substrate by pulse laser deposition (PLD), with optimum conditions for deposition as reported in [12, 13]. Two BZO-doped YBCO layers and the separating STO nano-layer were grown at temperature of 800^{o} C and laser frequency of 4 Hz using a 4 wt.% BZO-doped YBCO target prepared by a citrate-gel method described in detail elsewhere [15], and a STO target, respectively. The thickness of BZO-doped YBCO layers was 1.5 μm while the thickness of the insulating STO layer was 15 nm, 30 nm and 45 nm, respectively, with total film thickness slightly above 3 μm. For comparison, a single-layer film of BZO-doped YBCO was fabricated in the same conditions as the bilayer films.

The critical current density in magnetic fields along the *c* axis was determined from *DC* magnetisation loops of square 5 mm × 5 mm samples measured on a Quantum Design Magnetic Properties Measurement System (MPMS-XL) in DC field up to 4.5 T. The critical temperature (T_c) was measured on an MPMS-XL by recording temperature dependence of *AC* susceptibility in a small excitation field of 0.05 Oe. In magnetic fields of arbitrary orientation J_c was determined from the angle-dependent transport measurement on 550 μm long and 10 μm wide micro-bridges produced by conventional photolithography and chemical etching. The angle-dependent measurements have been done on a Quantum Design Physical Properties Measurement System (PPMS). Using the same equipment with a different set-up, pinning potentials were estimated from frequency-dependent *AC* susceptibility measurements, using a technique and data analysis as described in detail elsewhere [16]. The micro- and nanostructure of the samples was analysed by scanning electron microscopy (SEM, JEOL 7000) and transmission electron microscopy (TEM, Technai F20 operated at 200 kV). The cross-sectional TEM samples were prepared by focused-ion-beam milling (FIB) on a FEI Quanta 3D FEG.

3. Results and discussion

The superconducting properties of the bilayers were first examined by AC susceptibility measurements during slow temperature scans of 0.2 K/min. All films show sharp transition at high T_c of 89 K. Critical current density (J_c) for bilayer films with different thickness of insulating STO layer is shown in figure 1 in comparison with J_c of BZO-doped YBCO film of the same thickness deposited on Ag-decorated STO substrate. J_c was measured at temperature of 65 K and applied fields up to 4.5 T perpendicular to the film surface. This figure shows that the bilayer film with the thickness of the STO layer of 30 nm has the highest J_c in self-field, of about 3.86 MA/cm^2 while J_c's of the bilayer films with STO layer of 15 and 45 nm are of 2.86 and 3.53 MA/cm^2, respectively. The self-field J_c of all bilayer films at this temperature is higher than that of single layer BZO-doped YBCO film deposited on Ag-decorated STO substrate, which is about 2.67 MA/cm^2. J_c of bilayer films continues to be higher than that of single layer film in fields up to 1 T and the highest J_c is for the film with 30 nm-thick STO layer. However, in high applied fields, for example at 4 T, J_c of the single-layer film is the same as in the bilayer films with the thickness of STO layer of 30 and 45 nm (≈0.3 MA/cm^2). In high applied field perpendicular to the film surface, no improvement in J_c for bilayer films is observed in comparison with J_c of single-layer film.

In contrast, in applied fields parallel to the film surface, J_c of bilayer films obtained by transport measurement shows significant improvement in comparison with single-layer films, even when single layer films are thinner than the bilayer films as shown in figure 2. This figure compares J_c of the 3-μm bilayer film of the thickness of STO layer of 45 nm with 2-μm single-layer film on bare STO substrate and 2-μm single-layer film on the Ag-decorated substrate in applied fields up to 6 T and temperature of 77.3 K. Please note that due to problems related to the etching, we were unable to perform transport measurements on the 3-μm single layer film

prepared for comparison with bilayers. However, it is well known that for the same composition and growth conditions, J_c of a 3-μm film is smaller than that of a 2-μm film.

In self-field, J_c of the bilayer film (black stars) shows a 100% increase in comparison with J_c of the single-layer film (blue squares). In applied field of 6 T, J_c of the bilayer film (70 kA/cm^2) is 43% higher than that of single-layer film on bare substrate with J_c of 49 kA/cm^2, while J_c of the film on Ag-decorated substrate (red triangles) is in-between with the value of 59 kA/cm^2. It is obvious that STO layer separating two BZO-doped YBCO layers helps to increase J_c at 77 K both in self-field, and in fields up to 6 T parallel to the *ab*-plane.

It was earlier reported [7] that, in applied fields below 2.5 T, J_c in BZO-doped YBCO films is larger for magnetic fields applied along the *c* axis of YBCO, with a maximum of $J_c^c/J_c^{ab} = 2$, where J_c^c is critical current density for magnetic field along the c-axis and J_c^{ab} is critical current density for in-plane magnetic field. The same property can be seen in the bilayer film with 45 nm STO layer as shown by the angular dependence of J_c at temperature of 77.3 K presented in figure 3. In applied field of 0.6 T, J_c^c of the bilayer film at 0, 180 and 360^o is twice J_c^{ab} at 90 and 270^o. The J_c^c/J_c^{ab} ratio reduces to nearly 1 in applied field of 2.5 T and decreases further with increase of applied field, returning, for high fields to the "normal" situation in which $J_c^c/J_c^{ab} = 1/\gamma$, where γ is the YBCO anisotropy factor.

In an applied field of 2.5 T, J_c of all three samples: bilayer film, single layer on bare STO substrate and single layer on Ag-decorated STO substrate show low anisotropy of J_c with $J_c^c/J_c^{ab} \approx 1$ as shown in figure 4. Again, J_c for field along the *ab*-plane of the 3-μm bilayer film (blue squares) is higher than that of 2-μm single-layer film on Ag-decorated STO substrate (red circles) and of the single-layer film on bare substrate (black triangles). J_c for field along the *c* axis of the single-layer film on Ag-decorated substrate, however, is higher than that of bilayer film due to the thickness difference (it is well known that critical current density of YBCO decreases with increasing thickness, for thicknesses larger than several hundred nm). As shown

in figure 3, J_c for fields along the *c* axis of the bilayer is almost the same as in single-layer film on decorated substrate in applied field of 2.5 T.

In bilayers, for the field directions close to the *ab* plane, the peaks of J_c at 90^o and 270^o are split into two peaks as can be seen in figure 4. The cross-sectional TEM image of the bilayer film shown in figure 5 reveals the presence of fragments of planar defects parallel to the STO layer. If the average length of these fragments schematically shown in figure 6 by thick black lines is *L* and the average distance between them along *c*-axis is *l*, then the optimal angle φ at which pinning is strongest and segmented vortices are fit best to the planar defects is given by relation:

$$\tan(\varphi) = l/L. \qquad (1)$$

where Φ_0 is flux quantum and μ_0 is magnetic permeability of free space.

The TEM image in figure 5 allows rough estimates of *L* as 150 nm and *l* as 50 nm, which results in φ of approximately 18°. This value is close to that observed in figure 3 with positions of split maxima situated at $90°\pm\varphi$ and $270°\pm\varphi$.

The in-plane defects are only observed in the areas near the STO substrate and close to STO insulating layer, while the *c*-axis columns of BZO appear in the middle of BZO-doped YBCO layers, as shown in figure 7. The combination of the *ab*-plane and the *c*-axis defects act as active pinning sites maintaining high J_c not only in the direction of applied magnetic fields parallel to the *c* axis, but also for fields in the *a*-*b* plane, and this very peculiar pinning landscape is responsible for the split of the *ab*-plane peak in the $J_c(\Theta)$. Another origin of pinning in the BZO-doped YBCO films is in presence of Y_2O_3 nano-particles frequently observed in the bilayer sample and shown in figure 8. Although in literature [8] Y_2O_3 nano-particles were added to BZO-doped YBCO target to create more effective pinning, in our bilayer films the presence of Y_2O_3 nano-islands occurs naturally during film deposition.

The critical current density can also be calculated from AC susceptibility while a DC field is applied to the sample. From calculations of Brandt [17] on the flux penetration in superconductors with one dimension much smaller than the other two (disks, squares, stripes) in a perpendicular configuration (suitable for thin films with magnetic field perpendicular to the film surface), it was shown that the position h^* of the maximum in $\chi''(h_{ac})$ is related to the critical current density by the equation

$$J_c = \frac{h^*}{\alpha d}, \qquad (2)$$

where d is the film thickness and α is a constant between 0.8 and 0.9 that depends slightly on the geometry. An example of such frequency-dependent $\chi''(h_{ac})$ measured curves is shown in figure 8, for a bi-layer with 30nm- thick STO nanolayer, at 77.3 K and in 7 T DC field. From the frequency (time) dependence of critical current density, presented in figure 10 one can estimate the pinning potential, as shown in detail in Ref. 16. In brief, our data are very well described by a straight line in a double logarithmic plot in figure 10:

$$\ln J_c = a - b\ln\left(\frac{f_0}{f}\right). \qquad (3)$$

where f_0 is a macroscopic attempt frequency of about 10^6 Hz. The effective pinning potential, U_0 can be related [16] to the slope b in eq. (3) of our experimental data:

$$U_0 = k_B T\left(1+\frac{1}{b}\right). \qquad (4)$$

Using equation 4 and the data in figure 10, we estimated the effective pinning potential of the synergetic pinning centres in this film, at 77.3 K. The values (in K, k_B=1) are 389 (in 5 T), 271 K (in 6 T) and 176 K (in 7T). It is worth mentioning that, due to limitations in AC field amplitude (hence, in probing current), the experimental window in which such technique can be used is limited to high fields in thicker films, like in our case.

In conclusion, the combination of three methods is effective in increasing J_c of the film for magnetic fields oriented in both the *c*-axis and the *ab*-plane. The optimum thickness of the STO layer for increasing J_c is about 30 nm in applied fields lower than 1 T. Significant increase

of J_c for fields along the *ab*-plane of the bilayer film has been achieved. The presence of the fragments of *ab*-plane defects explains the split of the J_c peak in its dependence on magnetic field orientation close the *ab*-plane of YBCO. In perpendicular configuration, frequency-dependent AC susceptibility measurements allowed estimations of quite high effective pinning potentials in high magnetic fields.

Acknowledgements

This work has been supported by the COST Action MP 1201 "Nanoscale SuperConductivity: Novel Functionalities through Optimized Confinement of Condensate and Fields" and by Romanian Ministry of National Education and Research through Core Programme PN16-480102 "Synthesis and characterisation of nanostructured materials, thin films and hetherostructures"; through PCCA 138/2012; and through POC Project P_37_697 (28/01.09.2016) "Boron- and rare-earths-based advanced functional materials". V.S.D would also like to acknowledge the support for equipment of Nano and Energy Center, VNU-Hanoi University of Science, Vietnam.

References

[1] S. R. Foltyn, L. Civale, J. L. MacManus-Driscoll, Q. X. Jia, B. Maiorov, H. Wang and M. Maley, Nat. Mater., 6 (2007) 631.

[2] A. Crisan, S. Fujiwara, J. C. Nie, A. Sundaresan and H. Ihara, Appl. Phys. Lett., 79 (2001) 4547.

[3] A. Crisan, P. Badica, S. Fujiwara, J. C. Nie, A. Sundaresan, A. Iyo and Y. Tanaka, IEEE Trans. Appl. Supercond., 13 (2003) 3726.

[4] M. Ionescu, A. H. Li, Y. Zhao, H. K. Liu and A. Crisan, J. Phys.D: Appl. Phys., 37 (2004) 1824.

[5] J. L. MacManus-Driscoll, S. R. Foltyn, Q. X. Jia, H. Wang, A. Serquis, L. Civale, B. Maiorov, M. E. Hawley, M. P. Maley, and D. E. Peterson, Nat. Mater., 3 (2004) 439.

[6] M. M. Awang Kechik, P. Mikheenko, A. Sarkar, V. S. Dang, N. Hari Babu, D. A. Cardwell, J. S. Abell and A. Crisan, Supercond. Sci. Technol., 22 (2009) 034020.

[7] S. R. Foltyn, H. Wang, L. Civale, Q. X. Jia, P. N. Arendt, B. Maiorov, Y. Li, M. P. Maley, J. Mcmanus-Driscoll, Appl. Phys. Lett. 87 (2005) 162505.

[8] P. Mele, K. Matsumoto, T. Horide, A. Ichinose, M. Mukaida, Y. Yoshida, S. Horii, R. Kita, Physica C, 468 (2008) 1631.

[9] H. Zhou, B. Maiorov, S. A. Baily, P. C. Dowden, J. A. Kennison, L. Stan, T. G. Holesinger, Q. X. Jia, S. R. Foltyn, L. Civale, Supercond. Sci. Technol., 22 (2009) 085013.

[10] G. Ercolano, M. Bianchetti, S. C. Wimbush, S. A. Harrington, H. Wang, J. H. Lee, J. L. MacManus-Driscoll, Supercond. Sci. Technol. 24 (2011) 095012.

[11] L. Opherden, M. Sieger, P. Pahlke, R. Huhne, L. Schultz, A. Meledin, G. Van Tendeloo, R. Nast, B. Holzapfel, M. Bianchetti, J. L. MacManus-Driscoll, J. Hanish, Scientific Reports, 6 (2016) 21188.

[12] P. Mikheenko, A. Sarkar, V. S. Dang, J. L. Tanner, J. S. Abell, and A. Crisan, Physica C, 469 (2009) 798.

[13] P. Mikheenko, V. S. Dang, Y. Y. Tse, M. M. Awang Kechik, P. Paturi, H. Huhtinen, Y. Wang, J. S. Abell and A. Crisan, Supercond. Sci. Technol., 23 (2010) 125007.

[14] K. Develos-Bagarinao, H. Yamasaki and K. Ohki, J. Appl. Phys., 104 (2008) 063907.

[15] J. Raittila, H. Huhtinen, P. Paturi and Y. P. Stepanov, Physica C, 371 (2002) 90.

[16] A. Crisan, M.M. Awang Kechik, P. Mikheenko, V.S. Dang, J.S. Abell, P. Paturi, H. Huhtinen, Supercond. Sci. Technol., 22, (2009) 045014.

[17] E.H. Brandt, Physical Review B 49 (1994) 9024.

Figure captions

Fig 1. (Colour online). Field dependence of the critical current densities of bilayers composed of 1.5-μm BZO-doped YBCO films separated by STO layer of the thickness of 15 nm (S15, spheres) 30 nm (S30, triangles) and 45 nm (S45, stars) in comparison with J_c of a single-layer BZO-doped YBCO film (S0) on Ag-decorated STO substrate of the same thickness, at temperature of 65 K and applied fields parallel to the c axis of YBCO. Insert shows magnified area of figure 1 in applied fields between 0 and 1 T.

Fig 2. (Colour online). Field dependence of critical current density of 3–μm bilayer film (black stars), 2–μm single layer BZO-doped YBCO film on bare STO substrate (blue squares) and 2 μm single-layer BZO-doped YBCO film deposited on Ag-decorated STO substrate (red triangles) in applied field parallel to the *ab*-plane of YBCO at 77.3 K.

Fig 3. (Colour online). Angular dependence of critical current density of the bilayer film at 77.3 K, the value of applied magnetic fields is shown on the right hand side of each curve

Fig 4. (Colour online). Angular dependence of critical current density in applied field of 2.5 T and temperature of 77.3 K for 3-μm bilayer (blue squares), 2-μm single-layer on Ag-decorated substrate (red circles) and 2-μm single-layer on bare substrate (dark triangles). All films show low anisotropy of critical current density, close to 1.

Fig 5. Bright field cross-section TEM image of bilayer film around STO insulating layer, the *c* and *ab* axis of the film are marked by arrows.

Fig 6. (Colour online). Schematic representation of the pinning of vortices with their average direction along the red lines, the optimum pinning is achieved when the slope of vortex line is equal to the angle φ defined by the average length L of planar segments (thick black lines) and average distance between them l along the *c*-axis.

Fig 7. TEM image of extended BZO nano-rods in the YBCO far from the STO layer.

Fig 8. TEM image of an Y_2O_3 nano-particle in the matrix of YBCO

Fig. 9. (Colour online). Dependence of the out-of-phase susceptibility of the bi-layer film on the amplitude of AC field, for various frequencies (indicated in the image), in 7 T and at 77.3 K.

Fig. 10 (Colour online). Frequency-dependence of the critical current density of the bilayer film at 77.3 K, in fields of 5, 6, and 7 T

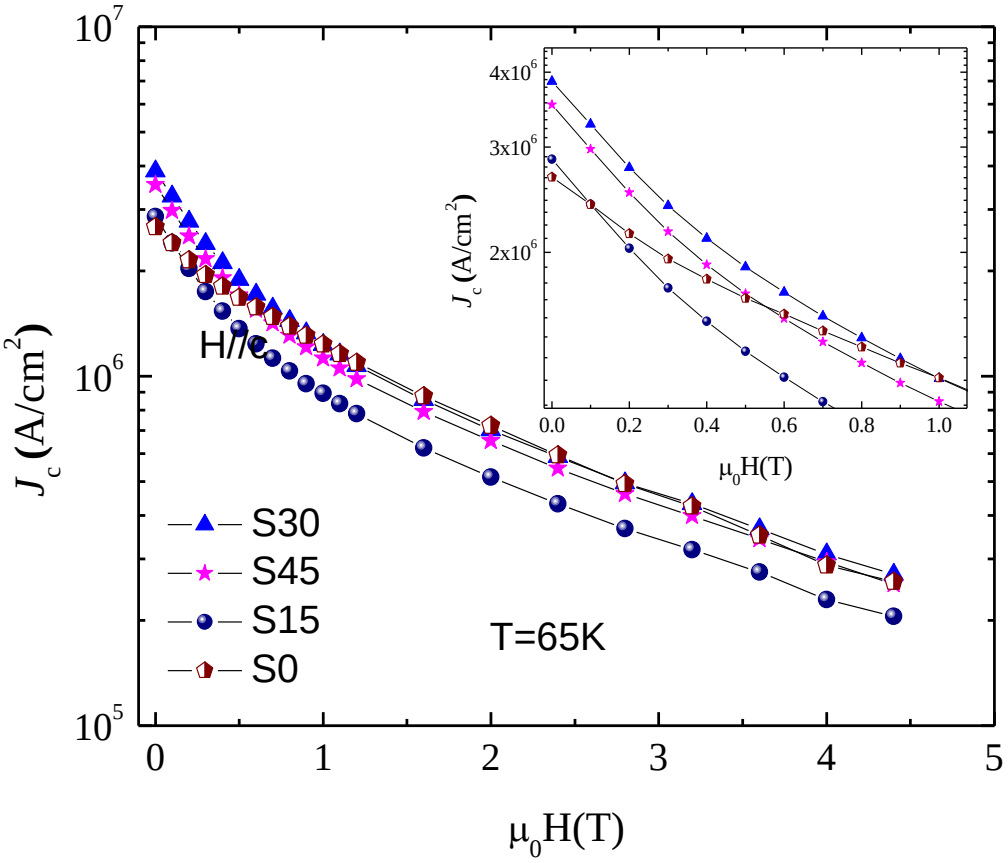

Fig 1. Crisan et al

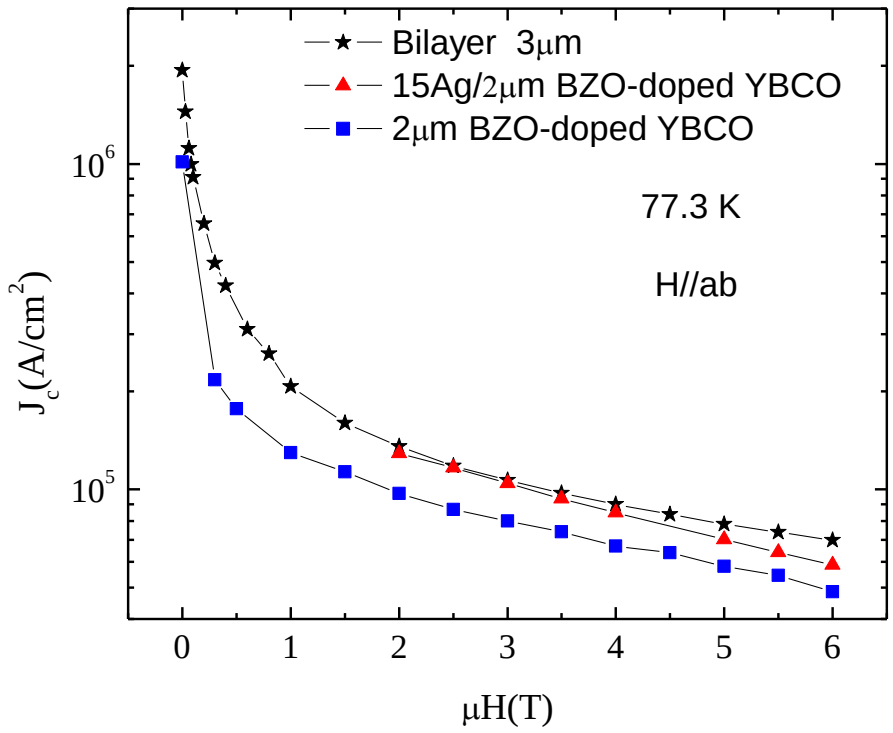

Fig 2. Crisan et al

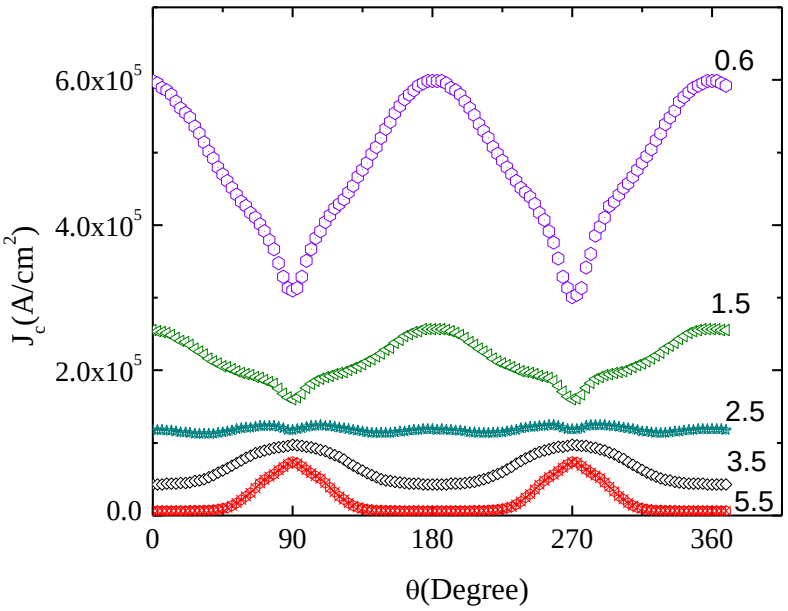

Fig 3. Crisan et al

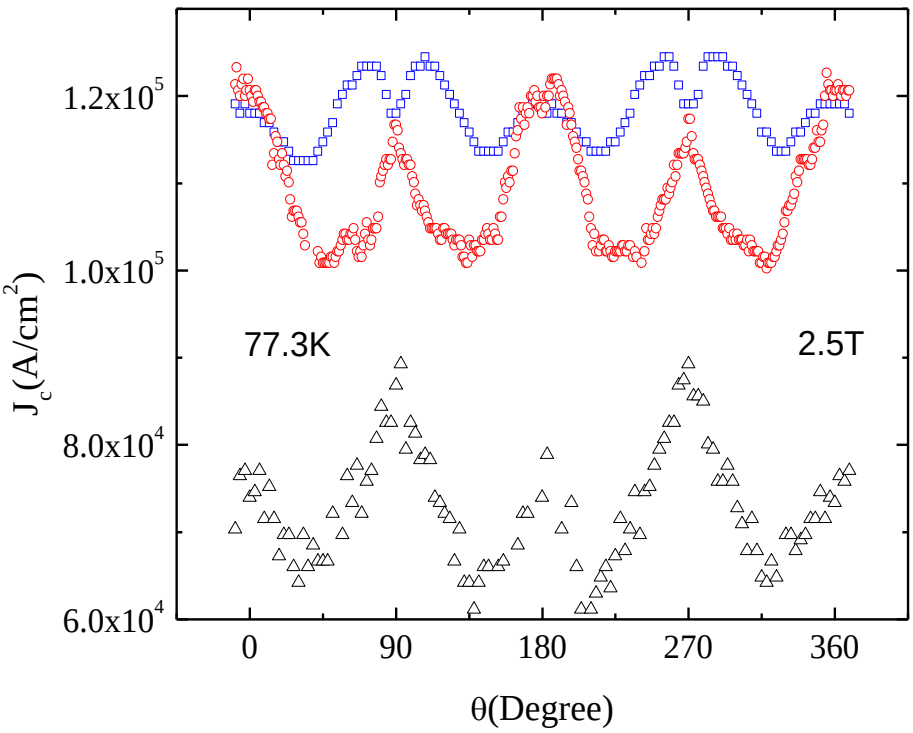

Fig 4. Crisan et al

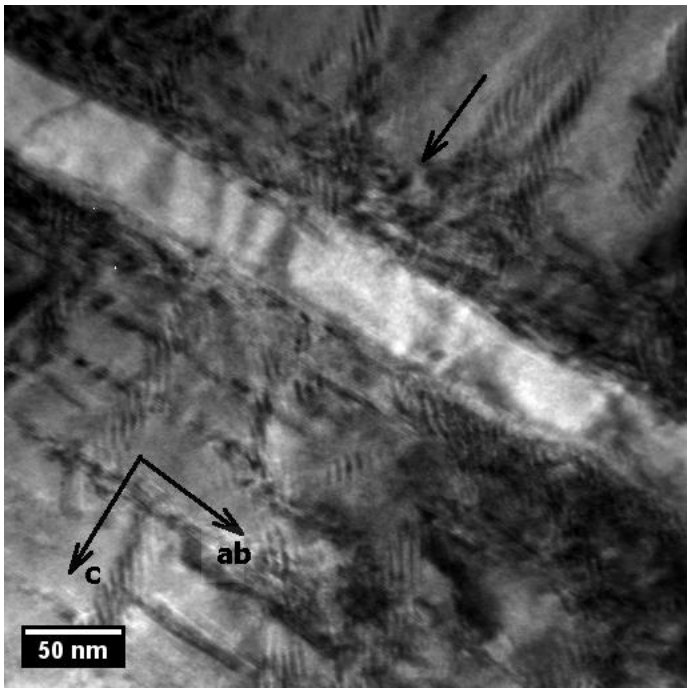

Fig 5. Crisan et al

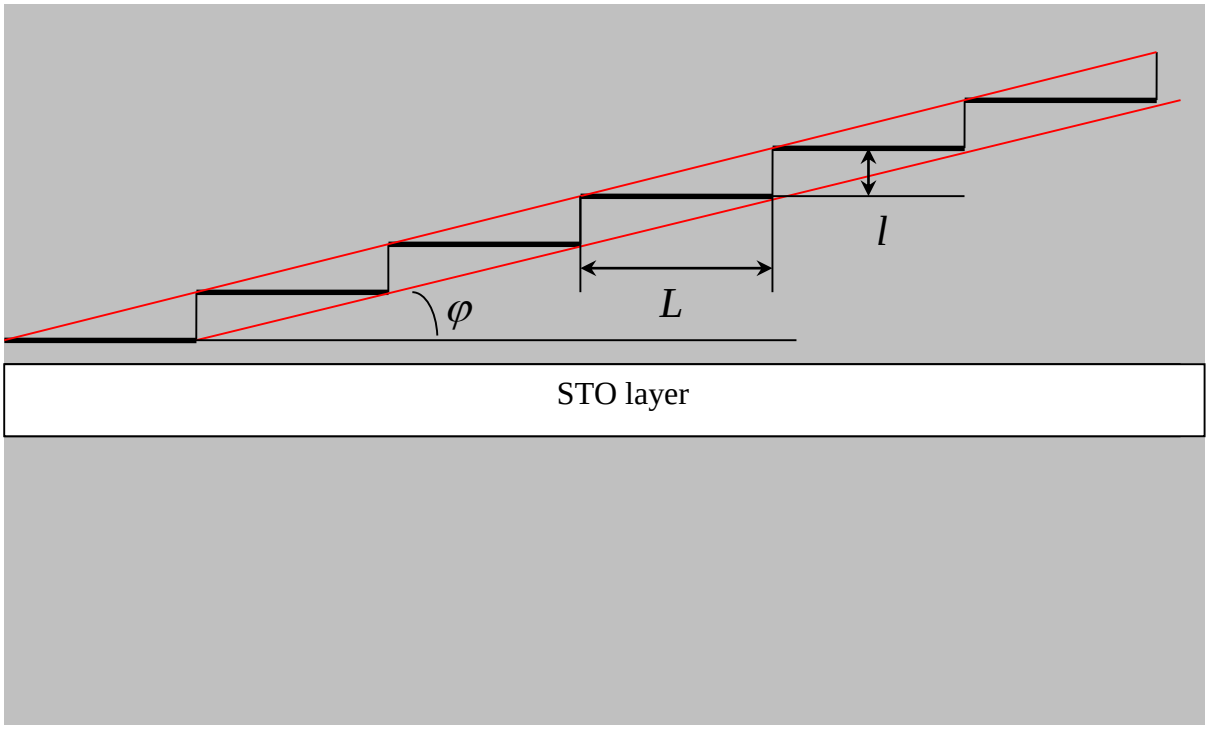

Fig 6. Crisan et al

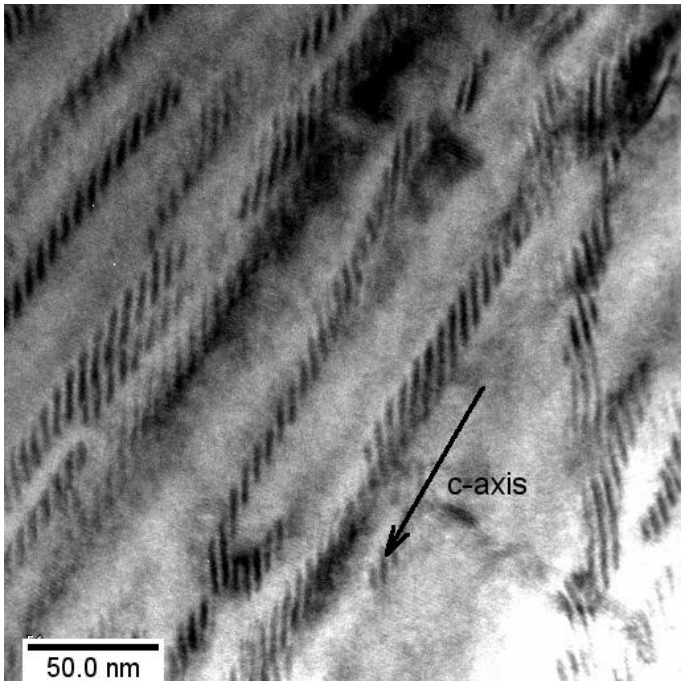

Fig 7. Crisan et al

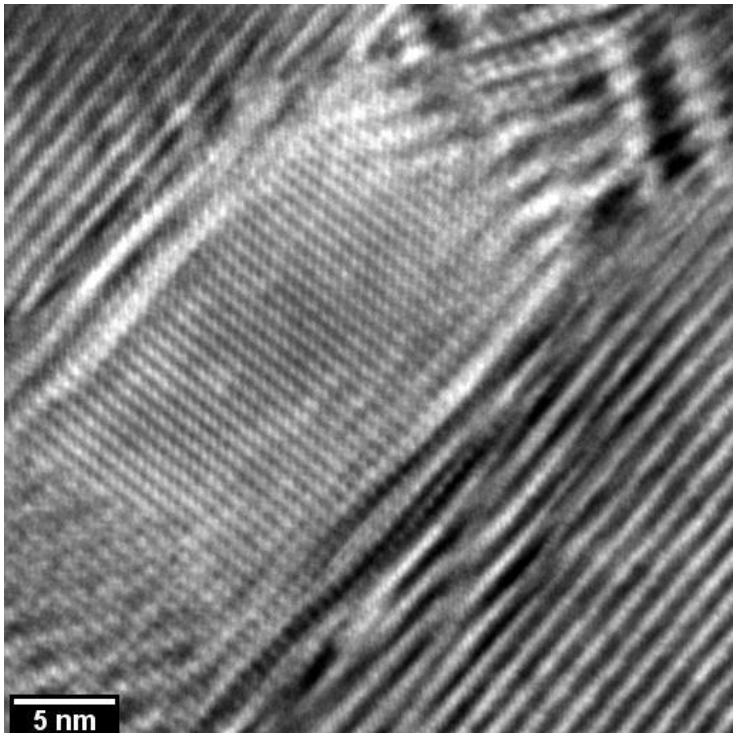

Fig 8. Crisan et al

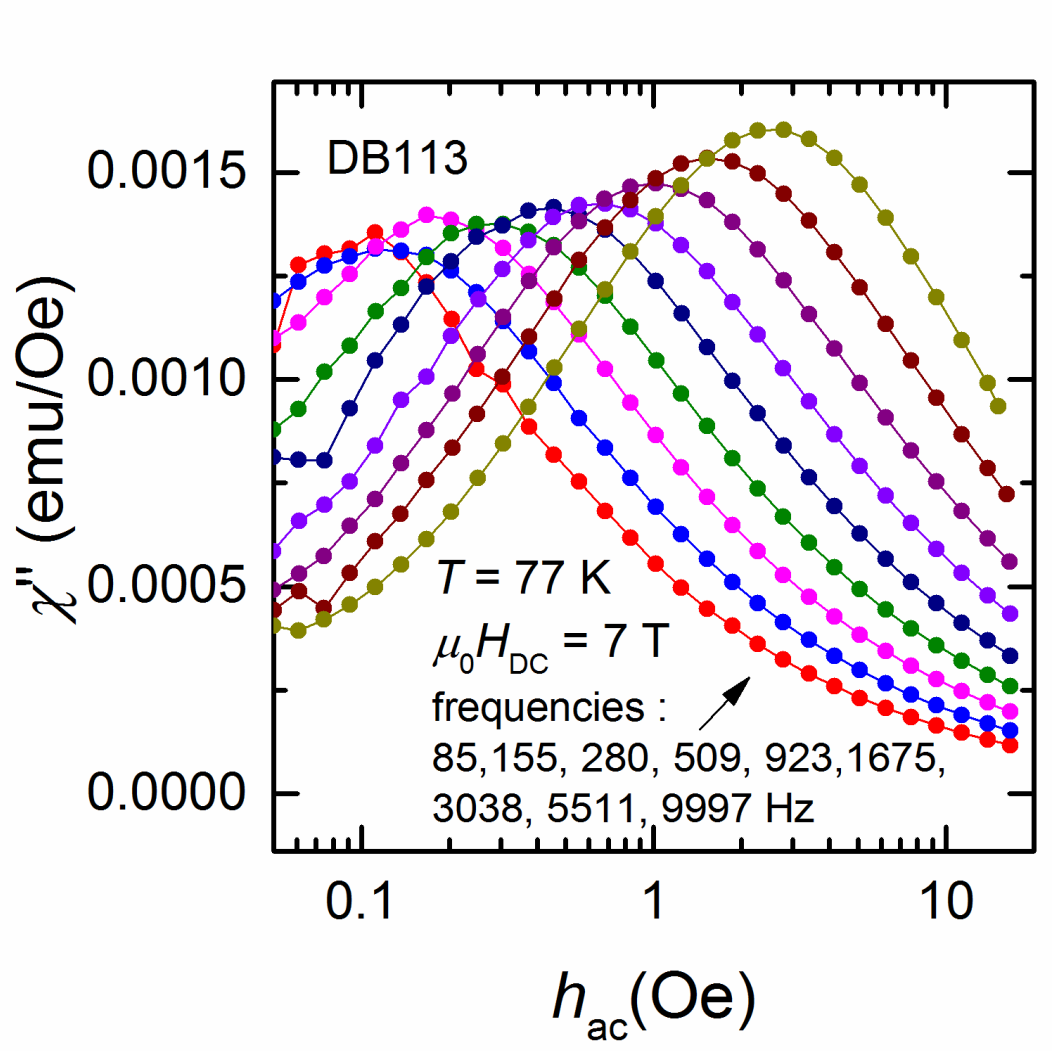

Fig. 9. Crisan et al.

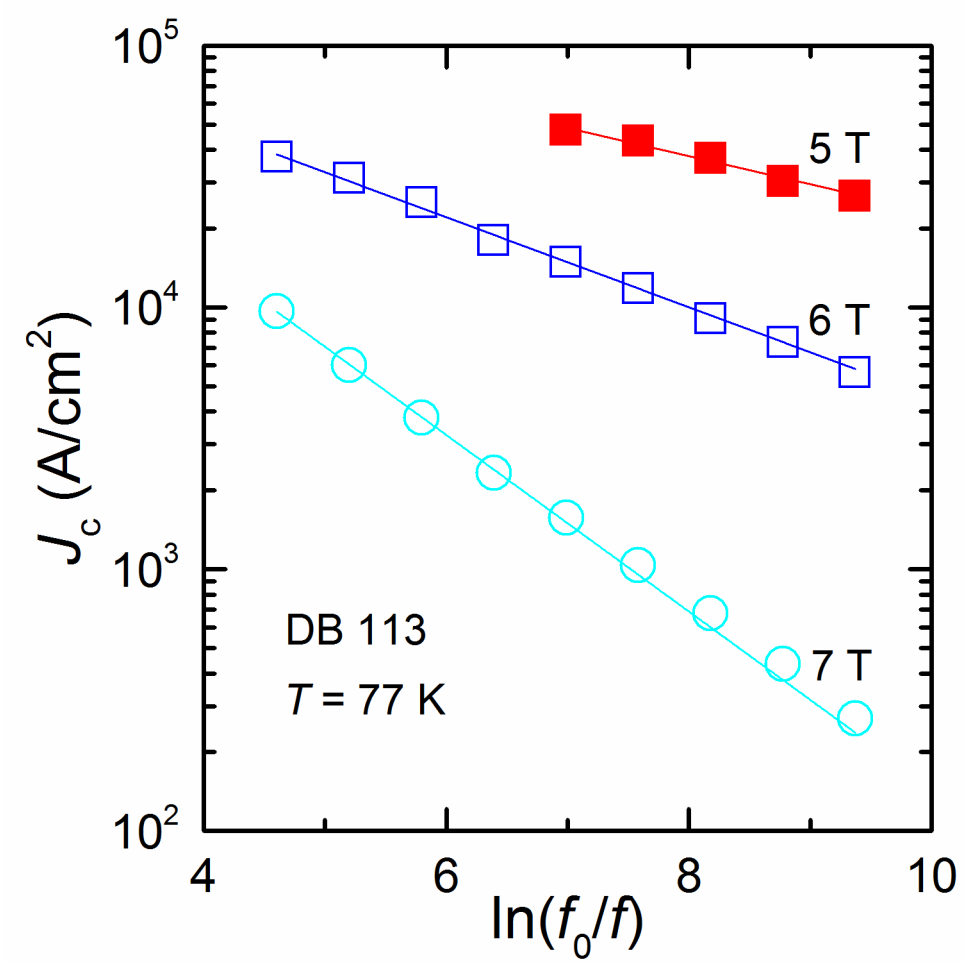

Fig. 10. Crisan et al.